

TESTING OF ANALOG PARTS OF ELECTRONIC EMBEDDED SYSTEMS WITH LIMITED ACCESS TO INTERNAL NODES

Zbigniew Czaja

Gdansk University of Technology, Faculty of Electronics, Telecommunications and Informatics, Department of Optoelectronics and Electronic Systems, Gdansk, Poland, zbczaja@pg.gda.pl

Abstract: A new class of multi-port methods based on extension of input-output two-port methods of soft fault diagnosis of passive elements in analog circuits is presented. It uses accessible internal nodes of the tested analog circuit for additional measurements of circuit time responses. Thanks to this, the fault resolution increases, that is we obtain better fault localization coverage.

Keywords: fault diagnosis, analog circuits, BIST

1. INTRODUCTION

The fast development of electronics and continuous increase of the complexity and variety of electronic circuits (chips, packets, microsystems and systems) create a large demand for methods of their testing and diagnosing. It implies big investigative interest in electronic diagnosis, especially of effective diagnosis methods of detection, localization and identification levels of hard (catastrophic) and soft (parametric) faults in analog circuits.

At present, the majority of electronic devices (embedded systems) is designed basing on digital circuits, but a lot of them requires difficult testing of analog components. It is estimated that 80% of testing costs is absorbed by analog functions of electronic devices. Hence, the industry looks for innovative testing methodologies which minimalize test costs and guarantee a high quality of products.

Techniques based on dedicated testing buses (e.g. IEEE 1149.4) or built-in testers (BIT or BIST) are the main global tendencies of investigation in this field.

The majority of elaborated BISTs are dedicated for analog to digital converters (ADCs) where usually BISTs have a more complex structure than the ADCs [1,2] and also for digital-to-analog converters (DACs) [3]. For analog filters and amplifiers generally three types of BISTs have been worked out:

- Based on sigma-delta modulators [4,5], where the BISTs consist of $\Sigma\Delta$ modulators, low-pass analog filters, ADCs, DACs and digital blocks.
- Based on the oscillation-test methodology [6-8], where the analog circuit is transformed into an oscillator by adding a feedback path and modifying the circuit either by adding or removing some passive components. Additionally a digital circuit which measures deviations of the frequency

of oscillation of the tested circuit, should be contained in the BIST.

- Based on a test strategy using power spectral analysis [9]. The tested circuit is stimulated by a noise generator, its response is sampled by an ADC and the estimation of the power spectrum density based on fast Fourier transform is realized by a digital signal processor (DSP).

The methods mentioned above need excessive structures built into the chip, which increases the price of testing, and they are characterized by a large requirement on computing power.

At present, electronic embedded systems form a large group of electronic devices. They have an own control-computational unit in the form of a microcontroller, a DSP or a system-on-chip (SoC).

Therefore, the author developed a new class of fault diagnosis methods [10-12] in which it is proposed to use internal hardware resources of control units (timers, PWMs, ADCs) to create reconfigurable BISTs for analog circuits, and to use their computing power to control the BISTs (realization of measurement procedures) and for calculations performed during the detection and localization procedures. In other words, in these methods own hardware resources and the computing power of control units enable to realize BISTs without additional circuits and without an infraction of the system structure, what minimizes the testing cost.

The elaborated methods belong to a class of input-output two-port methods in which a square impulse [10,11] or a square-wave signal [12] is applied to the input of the tested analog circuit and features of the response of the analog circuit are obtained by an internal ADC [10,12] or by an analog comparator and a timer [11] of the control unit.

The methods are ideally suitable for fault detection. However, fault localization of all elements and for circuits consisting of a large number of elements (more than 6) presents difficulties, because failures of elements mask themselves creating ambiguous groups, especially for circuits with tolerances, what is generally a disadvantage of input-output methods.

Thus, in the paper a new approach based on extension of input-output methods to the diagnosis of analog circuits with accessibility to internal nodes (modeled as multi-ports) is proposed. This solution, thanks to additional information obtained about the tested circuit from additional

measurement points, increases fault resolution to a level enabling almost complete fault localization.

2. DESCRIPTION OF THE METHOD

The idea of extension of input-output two-port methods to multi-port methods will be presented on an example of the method [10], in which the analog circuit is stimulated by a square impulse generated by the control unit (in this paper represented by the Atmega16 microcontroller of Atmel – Fig. 1), the response on the output of the circuit is sampled K times by the internal ADC at moments established by the internal timer of this control unit.

Thus, in the new method, sampling is realized in N nodes of the circuit, as shown in Fig. 1. The proposed solution also introduces no hardware excess, because every ADC of the microcontroller or the DSP has an 8- or 16-channel analog multiplexer.

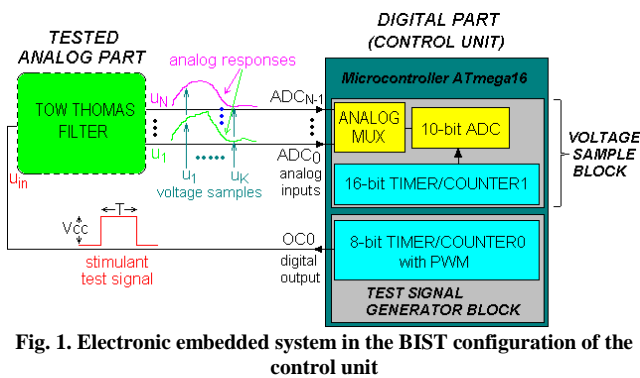


Fig. 1. Electronic embedded system in the BIST configuration of the control unit

The new method will be illustrated on the example of a low-pass Tow-Thomas filter (Fig. 2) stimulated by a square impulse with a duration time $T = 1$ ms and the amplitude set *a priori* to $V_{cc} = 5$ V.

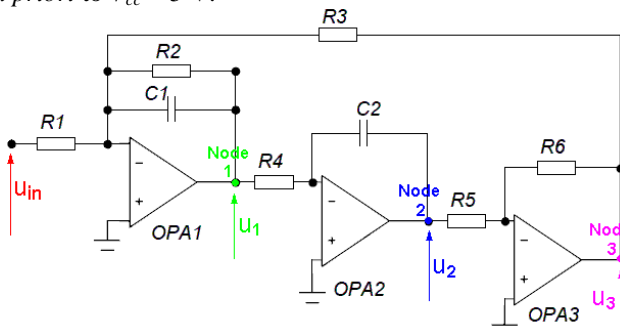


Fig. 2. Tested analog circuit – low-pass Tow-Tomas filter, where $R1 = R2 = R3 = R4 = R5 = R6 = 10$ k Ω , $C1 = 33$ nF, $C2 = 6.8$ nF

2.1. Idea of the new method

It was proved in [10] that the response of a linear electronic circuit to a square impulse for the assumed range of changes of values of different elements do not overlap each other in the output node, and the same in the internal nodes, which was also investigated in a simulated way (obviously, if failures of elements do not mask themselves).

Fig. 3 presents three sets of time responses of the circuit to the square impulse stimulation (Fig. 2) in respective nodes, where times $t_{n,k}$ are the k -th sample moments in the n node. Each set represents changes of the response of the circuit following from changes of the given element values

p_i , assuming that the remaining elements have their nominal values $p_{j,nom}$, where $i = 1, \dots, I$, I – the number of circuit elements. Therefore, it is possible to discern and to assign these responses to given elements (given an ambiguous group of elements) and to given element values [10] as shown in Fig. 3.

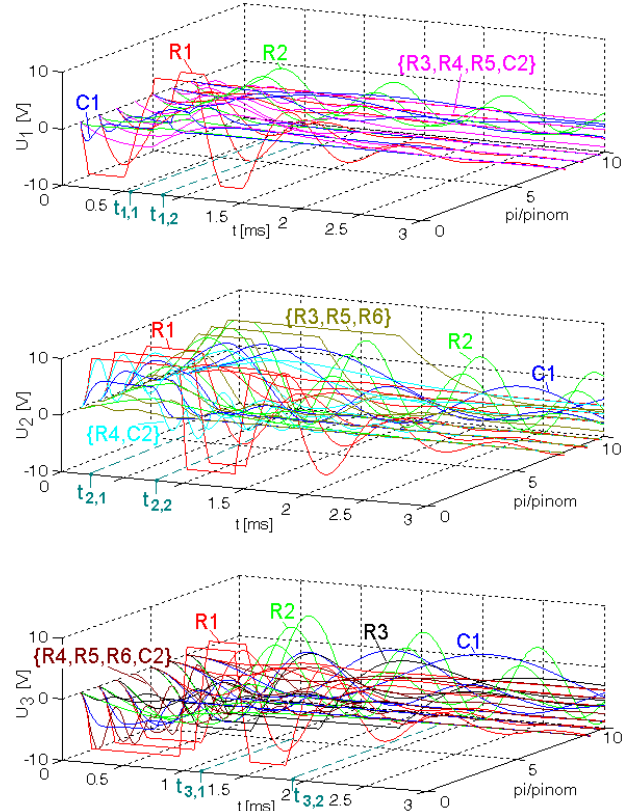


Fig. 3. Time responses of the Tow-Tomas filter (Fig. 2) for changes from 0.1 to 10 of nominal values of all elements in accessible nodes

If we make cross-sections of Fig. 3 at moments $t_{n,k}$ along the coordinate $p_i/p_{i,nom}$ assuming that values of the voltage sample at the moment $t_{n,k}(u_n)$ represent the $n-k$ coordinate, we will obtain a family of identification curves placed in the $K \cdot N$ dimensional measurement space. For $K = 2$ (as in [10]) and $N = 3$ we obtain a six-dimensional (6-D) space. Because it is difficult to draw the 6-D space in a plane, this space is presented in the form of three projections of identification curves in planes: $u_{n,1} - u_{n,2}$, where $n = 1, 2, 3$ (Fig. 4).

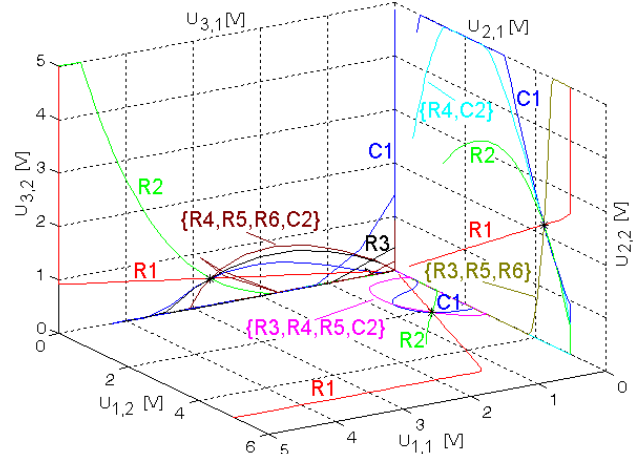


Fig. 4. The family of identification curves of the circuit in a 6-D measurement space presented as a composition of three measurement planes: $u_{n,1} - u_{n,2}$, where $n = 1, 2, 3$

Thus, we can describe the i -th curve in the form of the transformation:

$$T_i(p_i) = \sum_{n=1}^N \left(\sum_{k=1}^K u_n(p_i, t_{k,n}) \mathbf{i}_{n,k} \right) \quad (1)$$

where: $\mathbf{i}_{n,k}$ - is a coordinate vector along the k -axis, $k=1, \dots, K$, K - the number of voltage samples in each node, $u_n(p_i, t_{k,n})$ - value of the voltage sample at the moment $t_{k,n}$ in the n node (N - the number of accessible measurement nodes) for a change of value of the p_i element.

Hence, we can say that transformation (1) maps or "compresses" the sets of time responses in N nodes (Fig. 3) into the family of identification curves (Fig. 4) represented by the set of transformations $T_l = \{T_i(p_i)\}_{i=1, \dots, l}$. These curves are a graphical illustration of the behavior of the tested circuit resulting from deviation of its elements and they establish the fault dictionary.

2.2. Test Node Selection

Test node selection is to select a minimal node set $A_N = \{A_n\}_{n=1,2,\dots,N}$ to diagnose all possible faults. We assume that the output of the tested circuit is always accessible (the node with the number $N - A_N$). Hence, we have to determine $N-1$ internal accessible nodes for which a measurement access assures almost full fault localization coverage.

Criteria and methodology based on an analytic approach to the determination of internal accessible nodes will be explained on the example of analysis of node circuit function forms of the tested circuit (Fig. 2).

For the node A_1 we have the following node transfer function (2):

$$K_1(s) = \frac{-\frac{1}{R_1 C_1} s}{s^2 + \frac{1}{R_2 C_1} s + \frac{R_6}{R_3 R_4 R_5 C_1 C_2}} \quad (2)$$

It is seen that we have three coefficients dependent on elements values: $-1/(R_1 C_1)$, $1/(R_2 C_1)$, $R_6/(R_3 R_4 R_5 C_1 C_2)$. By analyzing forms of these coefficients, as shown in (2), we determine independent elements or independent sets of elements (clusters), that is elements which we can distinguish from other elements, considering all coefficients. E.g. for (2), the element C_1 is present in all coefficients but in different element configurations. Thus, this element is independent and deviations of its value can be directly presented in the form of the identification curve. Hence, excluding the C_1 element from coefficients, it is seen that also elements R_1 and R_2 occurring individually are independent. From the last coefficient it is seen (2) that we obtain the cluster $\{R_3, R_4, R_5, R_6, C_2\}$. These elements are not present in remaining coefficients and they can be treated as a "single element", thus it is impossible to distinguish whose element value change influences the node circuit function. Thus, this set of elements is represented only by one identification curve (Fig. 4). Summarizing, from node 1 we obtain independent elements R_1, R_2, C_1 and one cluster $\{R_3, R_4, R_5, R_6, C_2\}$.

The analysis is identical also for the circuit function in node 2. From (3) we determined the following independent elements: R_1, R_2, C_1 and two clusters: $\{R_3, R_5, R_6\}$, $\{R_4, C_2\}$.

$$K_2(s) = \frac{1}{s^2 + \frac{1}{R_2 C_1} s + \frac{R_6}{R_3 R_4 R_5 C_1 C_2}} \quad (3)$$

We can also make an analysis of the transfer function for the output node 3. From the voltage transmittance function (4):

$$K_3(s) = \frac{-\frac{R_6}{R_1 R_4 R_5 C_1 C_2}}{s^2 + \frac{1}{R_2 C_1} s + \frac{R_6}{R_3 R_4 R_5 C_1 C_2}} \quad (4)$$

we obtain independent elements R_1, R_2, R_3, C_1 and one cluster $\{R_4, R_5, R_6, C_2\}$.

Basing on these results (Table 1) we can choose internal accessible nodes.

Table 1. Summarizing independent element determination in accessible nodes of the tested circuit form Fig. 2.

Node	independent elements (clusters)
A_1	$R_1, R_2, C_1, \{R_3, R_4, R_5, R_6, C_2\}$
A_2	$R_1, R_2, C_1, \{R_3, R_5, R_6\}, \{R_4, C_2\}$
A_3	$R_1, R_2, C_1, R_3, \{R_4, R_5, R_6, C_2\}$

From Table 1 it is seen that we can choose only one internal node A_2 , (node A_3 is the output node) because the localization resolution for node A_1 is smaller than that for node A_2 , and for both nodes we have no different element configurations. Obviously, we can use the node A_1 which, thanks to additional measurement results, improves the localization accuracy.

Therefore, basing on independent element sets for nodes A_2 and A_3 we determine the final independent element set: $R_1, R_2, C_1, R_3, \{R_5, R_6\}, \{R_4, C_2\}$. Thus, we obtain a set greater than sets determined for individual nodes using two nodes simultaneously, that is we improved the localization resolution. This is the main advantage of the extension of input-output two-port diagnosis methods by addition of measurement access to internal nodes.

Obviously, to localize all elements we should add two nodes: the first node between R_5 and R_6 , the second one between R_4 and C_2 (see Fig. 2). In this case we have to analyze a 10-dimensional measurement space, which will make the presentation of the method illegible. Thus, the new method will be still presented on the example based on the measurement access to three nodes of the tested circuit.

2.3. Determination of stimulation parameters and sample moments

The mutual location and the shape (and also the length) of curves depend exclusively on the duration time T of the stimulus (the amplitude U_{in} is set *a priori* to V_{cc}) and on voltage sample moments $t_{n,k}$. The way of determination of the duration time T of the square impulse and sample moments $t_{N,k}$ for the output node A_N was described in [10].

To determine the voltage sample moments $t_{n,1}$ and $t_{n,2}$, in internal nodes 1,2, .. $N-1$ for which we obtain the best localization resolution, a coefficient of the localization

resolution $\lambda_{i,n}$ of the p_i element in particular nodes was introduced. For each n node, it is defined in the same way as in [10]:

$$\lambda_{i,n}(t_{n,k}) = \max_{j=1,\dots,L} \{u_n(p_{i,j}, t_{n,k})\} - \min_{j=1,\dots,L} \{u_n(p_{i,j}, t_{n,k})\} \quad (5)$$

where L – the number of discrete values of the element p_i in the assumed range from $0.1p_{i,nom}$ to $10p_{i,nom}$; each curve is represented by a set of L $q_{i,l}$ points ($T(p_{i,l}) \rightarrow q_{i,l}$), $t_{n,k}$ – the moment of the k -th sample in the node n .

The coefficient λ_n has the form:

$$\lambda_n(t) = \frac{1}{I} \sum_{i=1}^I \frac{\lambda_{i,n}(t)}{\max_{k=1,\dots,K} \{\lambda_{i,n}(t)\}} \quad (6)$$

Timings of these coefficients are shown in Fig. 5.

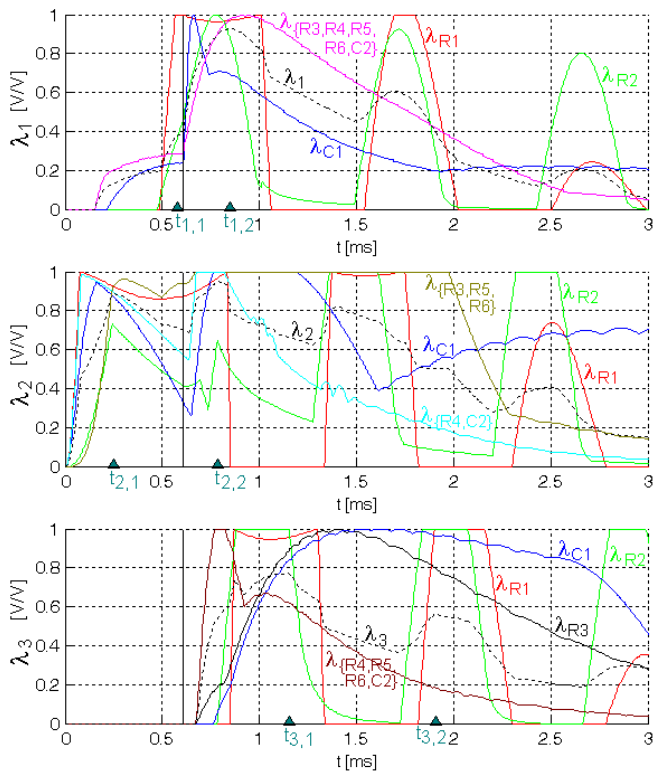


Fig. 5. Timings of the localization resolution coefficients for the Tow-Tomas filter (Fig. 2) for changes from 0.1 to 10 of nominal values of all elements in accessible nodes

The maximum value of λ_n represents the optimum sensitivity of the circuit voltage response measured in the node n to changes of values of all elements (Fig. 5). Thus we can define:

$$\lambda_{n,max1} = \max_{k=1,\dots,K_1, t_k \in (0,T)} \{\lambda_n(t_k)\} \quad (7a)$$

and

$$\lambda_{n,max2} = \max_{k=K_1+1,\dots,K, t_k \in (T,VT)} \{\lambda_n(t_k)\} \quad (7b)$$

where K_1 – the number of samples in the time range $(0, T)$.

So, the solution of (7) determines two moments of voltage samples for each node n :

$$\lambda_{n,max1} \rightarrow t_{n,1} \quad \text{and} \quad \lambda_{n,max2} \rightarrow t_{n,2} \quad (8)$$

Table 2 contains determined moments $t_{n,k}$ of two voltage samples ($K = 2$) for each of three nodes ($N = 3$) of the circuit from Fig. 2. In the Table, sample moments are also presented as the number of impulses counted by the 16-bit timer of the microcontroller (Fig. 1), where the system clock impulse has the period $t_{CLK} = 0.25 \mu\text{s}$.

Table 2. Moments $t_{n,k}$ of voltage samples in all nodes of the circuit from Fig. 2

$t_{n,k}$	$t_{1,1}$	$t_{1,2}$	$t_{2,1}$	$t_{2,2}$	$t_{3,1}$	$t_{3,2}$
[ms]	0.580	0.852	0.252	0.788	1.156	1.908
[*0.25 μs]	2320	3408	1008	3152	4624	7632

3. FAULT DIAGNOSIS PROCEDURES

The presented fault diagnosis method belongs to a simulation-before-test (SBT) class of methods, thus we can distinguish the following fault diagnosis procedures:

- Creation of the fault dictionary realized during the design of the embedded electronic system and only once for a given analog circuit.
- The measurement procedure based on the BIST created and controlled by the control unit.
- The fault detection and localization procedures also realized by the control unit.

3.1. Creation of the fault dictionary

The last procedure consists of two parts executed in turn: the detection procedure and the localization procedure. Thus, the creation of the fault dictionary was also divided into two parts. In the first part the data describing the nominal state of the tested analog circuit is generated. It is proposed to approximate the nominal areas representing this state (we assumed that $K=2$, as shown in Fig. 6) by N ellipses, because the n -th ellipse can be described only by coordinates of its foci $F_{n,1}$ and $F_{n,2}$ and the length $2a_n$ of the major axis. This description is ideally suitable for a fault detection algorithm, because we need to test that the sum of two distances between the measurement point and individual foci $F_{n,1}$ and $F_{n,2}$ of the ellipse is not greater than the length $2a_n$ of the major axis. This solution does not need complex calculations, thus it can be boldly implemented in such control units, especially in microcontrollers, which do not have great computing power.

The determination of parameters of the n -th approximation ellipse is realized by the following algorithm:

- M points with coordinates $(u_{n,1}^m, u_{n,2}^m)$ representing the n -th nominal area for the node n are generated using the Monte Carlo method.
- Based on these points, coefficients $B_{n,1}, B_{n,2}$ of the approximation straight line of the n -th nominal area given by the formula $u_{n,2} = B_{n,1}u_{n,1} + B_{n,2}$ are determined. This line passes through the nominal point P_{nom} . Its coefficients are calculated using the *polifit* function of Matlab.
- Next, the angle of inclination of the approximation straight line (simultaneously the angle of inclination of the approximation ellipse) is calculated: $\phi_n = \arctan(B_{n,1})$.
- The nominal area (the set of M points) $\{u_{n,1}^m, u_{n,2}^m\}_{m=1,\dots,M}$ is moved over by the vector $[-u_{n,1}^{nom}, -u_{n,2}^{nom}]$, where $u_{n,1}^{nom}, u_{n,2}^{nom}$ are coordinates of the nominal point P_{nom} .

(the centre of the ellipse). Next, this set is rotated about the angle ϕ_n :

$$\begin{aligned} u_{n,1}^{m*} &= u_{n,1}^m \cdot \cos(\phi_n) + u_{n,2}^m \cdot \sin(\phi_n) \\ u_{n,2}^{m*} &= -u_{n,1}^m \cdot \sin(\phi_n) + u_{n,2}^m \cdot \cos(\phi_n) \end{aligned} \quad (9)$$

In this way we obtain a set of points $\{u_{n,1}^{m*}, u_{n,2}^{m*}\}_{m*=1,\dots,M}$ which can be approximated by an ellipse with the centre (0,0) and focuses placed on the $u_{n,1}$ axis of the $u_{n,1} - u_{n,2}$ plane. It enables us to use basic formulas for the calculation of parameters of the ellipse.

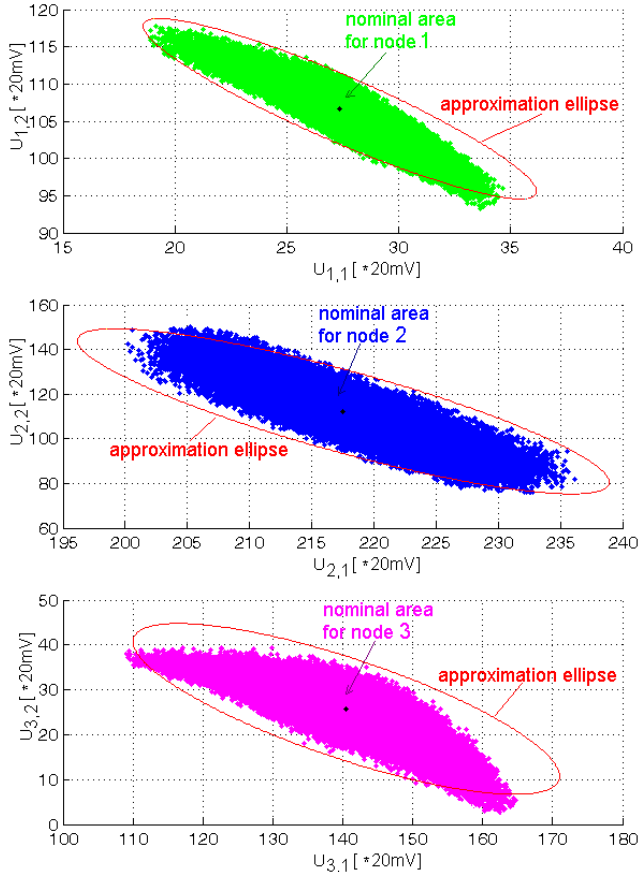


Fig. 6. Nominal areas for nodes accessible for measurement generated by the Monte Carlo method with assumption of 1% element tolerances

- The lengths of major $2a$ and minor $2b$ axes of the ellipse are determined from relationships:

$$\begin{aligned} a_n &= (\max_{m*=1,\dots,M} \{u_{n,1}^{m*}\} - \min_{m*=1,\dots,M} \{u_{n,1}^{m*}\}) / 2 \\ b_n &= (\max_{m*=1,\dots,M} \{u_{n,2}^{m*}\} - \min_{m*=1,\dots,M} \{u_{n,2}^{m*}\}) / 2 \end{aligned} \quad (10)$$

- Next, we calculate the distances between focuses and the centre of the ellipse: $c_n = \sqrt{a_n^2 + b_n^2}$.
- Finally, coordinates of focuses $F_{n,1}(u_{n,1}^{F1}, u_{n,2}^{F1})$ and $F_{n,2}(u_{n,1}^{F2}, u_{n,2}^{F2})$ of the ellipse are calculated from formulas:

$$\begin{cases} u_{n,1}^c = c_n \cdot \cos(\phi_n) \\ u_{n,2}^c = c_n \cdot \sin(\phi_n) \end{cases} \quad (11)$$

and

$$\begin{cases} u_{n,1}^{F1} = u_{n,1}^{nom} + u_{n,1}^c \\ u_{n,2}^{F1} = u_{n,2}^{nom} + u_{n,2}^c \end{cases} \quad \begin{cases} u_{n,1}^{F2} = u_{n,1}^{nom} - u_{n,1}^c \\ u_{n,2}^{F2} = u_{n,2}^{nom} - u_{n,2}^c \end{cases} \quad (12)$$

Using the taxi norm, the coefficient $2 \cdot a_n$ (the length of the major axis) was replaced by the equivalent coefficient $e_n = 2 \cdot a_n \cdot (\sin \phi_n + \cos \phi_n)$.

Thus, we obtain a description of all approximation ellipses: $\{(u_{n,1}^{F1}, u_{n,2}^{F1}), (u_{n,1}^{F2}, u_{n,2}^{F2}), e_n\}_{n=1,2,\dots,N}$. These ellipses are drawn in Fig. 6. In the figure the voltage values are presented in the form of the code which is compatible with the ADC conversion result contained in the 8-bit data register of the ADC (left adjustment result mode). Thanks to this, the ADC conversion results can be directly compared with the fault dictionary.

For the tested circuit the nominal point P_{nom} has coordinates (27, 107, 217, 112, 140, 26) [* 20mV]. Its approximation ellipses parameters are collected in Table 3.

Table 3. Approximation ellipse parameters (for 1% tolerances of R and 1% tolerances of C)

	$u_{n,1}^{F1}$ [*20mV]	$u_{n,2}^{F1}$ [*20mV]	$u_{n,1}^{F2}$ [*20mV]	$u_{n,2}^{F2}$ [*20mV]	e_n [*20mV]
n = 1	31	24	102	112	18
n = 2	230	205	107	117	43
n = 3	152	129	19	33	39

In the second part of the creation of the fault dictionary data describing I identification curves are created. Each i -th curve is approximated by a set of intervals, the endpoints of which are calculated from L values of p_i elements. Thus, the i -th curve is represented in the fault dictionary as a set of coordinates of L points $\{q_{i,l}\}_{l=1,\dots,L}$ ($q_{i,l} = T_i(p_{i,l})$) possibly evenly placed on it. The coordinates of each point are generated directly from the $p_{i,l}$ values using the Control Toolbox of Matlab. The relationship $p_i \rightarrow T_i(p_i)$ which transforms changes of p_i element values into the i -th curve placed in the $N \cdot K$ -dimensional measurement space, is nonlinear for all elements. Additionally, when we divide each curve in relation to the nominal point into two parts, the lengths of these parts have similar values. Thus, we make the following assumptions dealing with the layout of L approximation points on the i -th curve:

- A soft fault is an element value deviation in the range: $\langle \xi^{-1} \cdot p_{i,nom}, \xi \cdot p_{i,nom} \rangle$, where we assume in this paper that $\xi = 10$.
- The lengths of two curve parts have similar values, thus each part should be described by the same number of points, that is by the same number of $p_{i,l}$ element values in the interval $\langle \xi^{-1} \cdot p_{i,nom}, p_{i,nom} \rangle$ and in the interval $\langle p_{i,nom}, \xi \cdot p_{i,nom} \rangle$.

Thus, based on these assumptions and simulation results, the logarithmic expansion of elements values $\{p_{i,l}\}_{l=1,\dots,L}$ in the assumed range $\langle \xi^{-1} \cdot p_{i,nom}, \xi \cdot p_{i,nom} \rangle$ was chosen ($\text{logspace}(\xi^{-1} \cdot p_{i,nom}, \xi \cdot p_{i,nom}, L)$ function of Matlab). In spite of the fact that this solution is very simple, it gives a good even layout of $\{q_{i,l}\}_{l=1,\dots,L}$ points on the i -th curve.

Hence, the family of identification curves is represented by the coordinate set: $\{(\{u_{n,k}^{i,l}\}_{n=1,\dots,N, k=1,\dots,K}; i=1,\dots,I, l=1, \dots, L), \Gamma\}$, where coefficient Γ defines the concentration of additional points $\{q_{i,l}^{\gamma}\}_{\gamma=0,1,\dots,\Gamma-1}$ approximating the i, l -th interval with

$q_{i,l}$ and $q_{i,l+1}$ endpoints. This solution decidedly simplifies calculations of the distance between the measurement point and the i,l -th interval, what will be presented by a description of the localization algorithm.

Finally, we obtain the following form of the fault dictionary; $\{(u_{n,1}^{F1}, u_{n,2}^{F1}), (u_{n,1}^{F2}, u_{n,2}^{F2}), e_n\}_{n=1,2,\dots,N}$, $(\{u_{n,k}^{i,l}\}_{n=1,\dots,N, k=1,\dots,K; i=1,\dots,I, l=1,\dots,L}, T)$. The size of the fault dictionary is equal to $S = (2 \cdot K + 1) \cdot N + (N \cdot K \cdot I \cdot L + 1)$. Therefore, in the considered example $I = 8, N = 3, K = 2$ and for $L = 32$ ($L = 64$) the fault dictionary occupies $S = 1744$ bytes (3472 bytes) of the program memory of the control unit. Thus, it is small in comparison with the size of the program memory of a typical microcontroller (e.g. Atmega16 has 16KB of program memory); this is also an advantage of the proposed diagnosis method.

At the end of the fault dictionary creation part, the fault dictionary is converted to the form shown in Listing 1 and placed into the program code of the microcontroller.

```
#define N 3
#define K 2
#define NK N*K

typedef unsigned char uint8;

/* fault dictionary - detection part*/

const uint8 u_nom[NK] = {27,107,217,112,140,26};
const uint8 u_F1[NK] = {31,230,152, 24,205,129};
const uint8 u_F2[NK] = {102,107,19, 112,117,33};
const uint8 e_n[N] = {18,43,39};
```

Listing 1. Fragment with the detection part of the fault dictionary written in the ANSI C code

3.2. The measurement procedure

The measurement procedure, the same as in [10], is executed during self-testing of the embedded system. The BIST consists of the following internal devices of the exemplary Atmega16 microcontroller [13] (Fig. 1):

- 8-bit timer generating the square impulse stimulating the tested analog circuit.
- An ADC with the analog multiplexer, which allows to sample the voltage of the time response in N accessible nodes.
- 16-bit timer triggering the ADC at established moments $t_{n,k}$.

The microcontroller controls this procedure according to the *measurement* function included in its program memory [10]. This procedure is extended by the service of switching of the ADC between nodes, as shown in Listing 2.

```
uint8 n, k, u_meas[NK];
int t_sample[NK] = {290,426,126,394,578,961};
// prescaler set 1:8 for fclk = 4MHz
for(n = 1; n <= N; n++)
{
  ADMUX &= 0xF8; // Selection of the (n - 1)
                // analog channel
  ADMUX |= (n - 1); // from 0 .. 7 channels

  for(k = 1; k <= K; k++)
  {
    u_meas[n*k - 1] = measurement(t_sample[n*k - 1]);
  }
}
```

Listing 2. The multi-node measurement procedure in the ANSI C code

The *measurement()* function algorithm was described in detail in [10]. The function returns the voltage sample result to the byte variable $u_meas[n*k - 1]$, and the ADC is triggered at the moment $t_sample[n*k - 1] * 4 \mu s$. Analyzing Listing 2 it is seen that this function is repeated $N \cdot K$ times by using two loops “for”. In the external loop “for” repeating N times we switch the input of the ADC to the n node using the analog multiplexer. The internal loop “for” is responsible for sampling K times the voltage in the n node.

3.3. The fault detection and localization procedures

Information obtained about the tested circuit in the form of the measurement point P_{meas} with coordinates $(\{u_{n,k}^{meas}\}_{n=1,\dots,N, k=1,\dots,K})$ is sent to a function realizing the fault detection and localization procedures.

At the beginning, the fault detection procedure based on the measurement point and the fault dictionary with data describing respective nominal areas performs a fault detection. The control unit checks: if the measurement point $P_{meas}(u_{n,1}^{meas}, u_{n,2}^{meas})$ is contained simultaneously inside all N approximation ellipses described by the data set $\{(u_{n,1}^{F1}, u_{n,2}^{F1}), (u_{n,1}^{F2}, u_{n,2}^{F2}), e_n\}_{n=1,2,\dots,N}$. The following set of inequalities is calculated and tested (basing on the taxi norm):

$$\begin{cases} \sum_{k=1}^2 (|u_{1,k}^{meas} - u_{1,k}^{F1}| + |u_{1,k}^{meas} - u_{1,k}^{F2}|) \leq e_1 \\ \sum_{k=1}^2 (|u_{2,k}^{meas} - u_{2,k}^{F1}| + |u_{2,k}^{meas} - u_{2,k}^{F2}|) \leq e_2 \\ \dots \\ \sum_{k=1}^2 (|u_{N,k}^{meas} - u_{N,k}^{F1}| + |u_{N,k}^{meas} - u_{N,k}^{F2}|) \leq e_N \end{cases} \quad (13)$$

If the inequalities (13) are fulfilled (the measurement point is placed inside all ellipses), the tested analog part is fault-free and the fault diagnosis procedure is finished.

To test quantitatively the approximation of nominal areas by ellipses and also the effectiveness of the detection procedure, the Fault Detection Covering coefficient was introduced:

$$FDC_n[\%] = \frac{m_n}{M_n} \cdot 100\% \quad (14)$$

where: m_n – the number of corrected detected measurement points for the n -th node, M_n – the number of all generated points representing the nominal area of the n -th node and introduced to the detection algorithm.

Simulation results basing on the Monte Carlo method of FDC_n coefficients for 1% resistors tolerance and for 1%, 2.5% and 5% capacitor tolerances are collected in Tables 3, 4 and 5.

Table 3. FDC_i for 1% tolerances of R and 1% tolerances of C

Nominal area	n = 1	n = 2	n = 3	For all nodes
taxi FDC_n [%]	99.85	98.4	99.7	98.1
Euclid FDC_n [%]	99.2	96	99.5	95.7

Table 4. FDC_i for 1% tolerances of R and 2.5% tolerances of C

Nominal area	n = 1	n = 2	n = 3	For all nodes
taxi FDC_n [%]	99.7	99.35	99.1	98.9
Euclid FDC_n [%]	98.7	97.5	98.8	96.65

Table 5. FDC_i for 1% tolerances of R and 5% tolerances of C

Nominal area	n = 1	n = 2	n = 3	For all nodes
taxi FDC_n [%]	99.8	99.65	98.2	98.15
Euclid FDC_n [%]	99.05	98.4	97.7	96.6

Tables contain results based on taxi norm calculations (13), and also for comparison, based on Euclid's norm.

It is seen that the detection procedure works correctly for 1% tolerances of all elements (for all nodes $FDC_n > 98\%$), as shown in Table 3. This coefficient is even better for higher tolerance values of capacitors (Tables 4 and 5), because the nominal areas "fill" better the approximation ellipses. Thus, we can say that in spite of simple models of nominal areas we obtained a high level of fault detection correctness.

If the fault detection procedure detects a fault, the localization procedure of soft single faults of passive elements is executed. A search for a fault consists of the following steps described below:

- The set of distances $d_l = \{d_i\}_{i=1,\dots,l}$ between the measurement point P_{meas} and all l identification curves is determined. It is assumed that the calculation of the distance d_i between point P_{meas} and i -th curve is realized in the following way:
 - The set of distances $d_{i,l} = \{d_{i,l}\}_{l=1,\dots,L}$ between point P_{meas} and L points $q_{i,l}$ approximating the particular i -th curve is determined.
 - The $d_{i,min} = \min\{d_{i,l}\}_{l=1,\dots,L}$ value points to the nearest point $q_{i,l}$ and $d_{i,min,next} = \min\{\{d_{i,l}\}_{l=1,\dots,L} - d_{i,min}\}$ value points to the next nearest point $q_{i,l+1}$ in relation to the point P_{meas} .
 - These points are endpoints of the i,l -th interval of the i -th curve situated nearest to the point P_{meas} . Thus, we have to calculate the distance $d_{i,l}$ between this interval and the point P_{meas} . We find an approximation value of this distance in the next steps, in the way shown in Fig. 7:

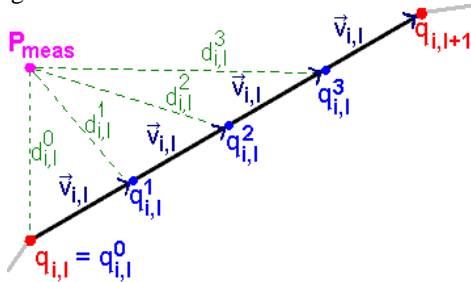


Fig. 7. Idea of determination of the distance between the measurement point P_{meas} and the i,l -th interval with endpoints $q_{i,l}$ and $q_{i,l+1}$

- The vector $v_{i,l}$ is assigned $v_{i,l} = \{v_{n,k}\}_{n=1,\dots,N, k=1,\dots,K}$

$$= \left(\left\{ \frac{u_{n,k}^{i,l} - u_{n,k}^{i,l+1}}{\Gamma} \cdot \mathbf{i}_{n,k} \right\}_{k=1,\dots,K; n=1,\dots,N} \right)$$
 where the coefficient $\Gamma = 2^\rho$, ($\rho = 1, 2, \dots, 8$) defines the concentration of points $\{q_{i,l}^\gamma\}_{\gamma=0,1,\dots,\Gamma-1}$ approximating the i,l -th interval (see Fig. 7) and $\mathbf{i}_{n,k}$ is a coordinate vector along the $n-k$ -axis.
 - We determine these points by successively moving the point $q_{i,l}$ about the vector $v_{i,l}$: $q_{i,l}^\gamma = q_{i,l} + \gamma \cdot v_{i,l}$, where $\gamma=0,1,\dots,\Gamma-1$ (Fig. 7).

- Next, we calculate distances $\{d_{i,l}^\gamma\}_{\gamma=0,1,\dots,\Gamma-1}$ between the set of points $\{q_{i,l}^\gamma\}_{\gamma=0,1,\dots,\Gamma-1}$ and the point P_{meas} .
- At the end, we determine $d_l = \min\{d_{i,l}^\gamma\}_{\gamma=0,1,\dots,\Gamma-1}$.
- The minimum distance d_{min} from the set d_l is assigned: $d_{min} = \min\{d_i\}_{i=1,\dots,l}$. Therefore, the index i for which we obtained the minimum distance d_{min} is the index of the faulty element.

The algorithm describing the steps of the distance determination between measurement point P_{meas} and the i,l -th interval is shown in Fig. 8.

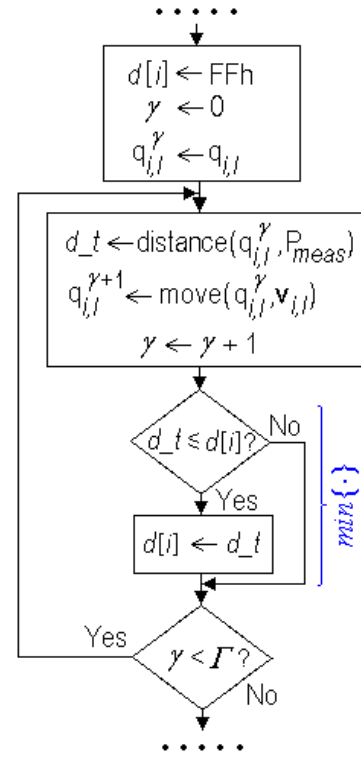


Fig. 8. Fragment of the localization algorithm with determination of distance between measurement point P_{meas} and the i,l -th interval

For simplifying Fig. 8 it was assumed that $q_{i,l}^\gamma$ represents the table variable $u_{il_g}[NK]$, $q_{i,l}$ the table variable $u_{il}[NK]$, $v_{i,l}$ the table variable $v_{il}[NK]$ and P_{meas} the table variable $u_{meas}[NK]$, where the constant value $NK = N \cdot K$.

Therefore, Fig. 8 presents the algorithm implementation of the idea shown in Fig. 7. At the beginning of the algorithm we initialize variables $d[i]$, γ and the point $q_{i,l}^\gamma$ represents the endpoint $q_{i,l}$ of the interval. In the loop repeated Γ times, we calculate the distance between the point $q_{i,l}^\gamma$ and the point P_{meas} using the $distance()$ function. Then the point $q_{i,l}^\gamma$ is moved to the next position by the vector $v_{i,l}$. This operation is realized by the $move()$ function. After this operation the content of the variable $d[i]$ is compared with the content of the temporary variable d_t . If the value of the d_t is smaller than the value of the $d[i]$, the variable $d[i]$ is actualized by the value of the d_t , because we assumed that the smallest distance from all distances $d_{i,l}^\gamma$ between P_{meas} and all points $q_{i,l}^\gamma$ is the distance between P_{meas} and the interval. So, we realize the $min\{\cdot\}$ function in a simple way using only one integer variable. Finishing this fragment of the localization algorithm the variable $d[i]$ keeps

the distance d_i between the measurement point P_{meas} and i -th approximation curve.

Thus, these procedures finish the self-testing of the analog circuit of the electronic embedded system run by the control unit. The fault diagnosis result can be shown on any display of the device or can be sent via any interface e.g. to the main computer.

One should underline the fact that this self-testing approach of analog circuits consisting of measurement, detection and localization procedures should be treated as part of full self-testing of the electronic embedded system, where the software, memories, the microprocessor core, digital circuits and remaining important components of the system are tested. Hence, procedures of self-testing of analog circuits and the fault dictionary were elaborated with regard to minimal occupation of the program memory space of the control unit and minimal requirement on computing power, what was presented in the paper.

4. CONCLUSIONS

A novelty of the proposed approach is the extension of input-output two-port methods of soft fault diagnosis of passive elements elaborated by the author to a new class of multi-port methods, which base on additional measurements of circuit time responses made in internal accessible nodes of the tested analog circuit. This solution, among other things causes an N -times increase of the size of the measurement space with the family of identification curves (N – the number of accessible nodes). It implies greater distances between curves and, in consequence, better fault resolution, which gives better fault localization coverage.

The paper also proposes:

- An extension of determination of voltage sample moments to accessible internal nodes.
- A new methodology of determination of internal accessible nodes based on an analysis of the form of the node circuit transmittance function.
- New algorithms of creation of the fault dictionary, where nominal areas are represented by approximation ellipses and identification curves are approximated by sets of intervals. This solution allows to obtain a small size of the fault dictionary and simultaneously good representation of circuit proprieties.
- Adaptation of the measurement procedure and the BIST for the new multi-port diagnosis method by addition of the service of the internal analog multiplexer of the control unit.
- New modified detection and localization procedures, where the fault detection bases on testing that the measurement point is inside all approximation ellipses, and the fault localization bases on determination of the minimal distance from calculated distances between the measurement point and the sets of intervals representing respective identification curves.

REFERENCES

[1] Vecera I., Vrba R.: "An algorithmic A/D switched-current converter for smart signal digitization with self-test features", *Measurement*, Vol. 35, Issue 2, pp. 153-160, March 2004.

[2] Venuto D., Reyneri L.: "Fully digital strategy for fast calibration and test of SD ADCs", *Microelectronic Journal*, Vol. 38, Issue 4-5, pp. 474-481, April 2007.

[3] Yun-Che W., Kuen-Jong L.: "A current-mode BIST structure of DACs", *Measurement*, Vol. 31, Issue 3, pp. 147-163, April 2002.

[4] Raczkowycz J., Mather P., Saine S.: "Using a sigma-delta modulator as a test vehicle for embedded mixed-signal test", *Microelectronic Journal*, Vol. 31, Issue 8, pp. 689-699, August 2000.

[5] Prenat G., Mir S., Vazques D., Rolindez L.: "A low-cost digital frequency testing approach for mixed-signal devices using $\Sigma\Delta$ modulation", *Microelectronic Journal*, Vol. 36, Issue 12, pp. 1080-1090, December 2005.

[6] Arabi K., Kamińska B.: "Oscillation-Test Methodology for Low-Cost Testing of Active Analog Filters", *IEEE Transactions on Instrumentation and Measurement*, Vol. 48, No. 4, pp. 798-806, August 1999.

[7] Toczek W., Zielonko R.: "A measuring systems for fault detection via oscillation", *Proceedings of the XVI IMEKO World Congress*, Vol. 6, pp. 287-292, Vienna, Austria, 2000.

[8] Huertas G., Vazques D., Peralias E., Rueda A., Huertas J. L.: "Oscillation-based test in oversampled $\Sigma\Delta$ modulators", *Microelectronic Journal*, Vol. 33, Issue 10, pp. 799-806, October 2002.

[9] Negreiros M., Carro L., Susin A. A.: "Testing analog circuits using spectral analysis", *Microelectronic Journal*, Vol. 34, Issue 10, pp. 937-944, October 2003.

[10] Czaja Z.: "A diagnosis method of analog parts of mixed-signal systems controlled by microcontrollers", *Measurement*, Vol. 40, Issue 2, pp. 158-170, February 2007.

[11] Czaja Z.: "A fault diagnosis method of analog electronic circuits for mixed-signal systems controlled by microcontrollers", *Proceedings of the IEEE Instrumentation and Measurement Conference, IMTC 2006*, pp. 1211-1216, Sorrento, Italy, April 2006.

[12] Czaja Z.: "Using a square-wave signal for fault diagnosis of analog parts of mixed-signal embedded systems controlled by microcontrollers", *Proceedings of the IEEE Instrumentation and Measurement Conference, IMTC 2007*, Warsaw, Poland, May 2007.

[13] Atmel Corporation: "8-bit AVR microcontroller with 16k Bytes In-System Programmable Flash, ATmega16, ATmega16L", PDF file, available at: <http://www.atmel.com>, 2003.